Eur. Phys. J. A **13**, 419–428 (2002)
DOI 10.1140/epja/iepja1299

THE EUROPEAN PHYSICAL JOURNAL A

Experimental investigation of the level density in highly excited nuclei around ^{208}Pb

M. Lunardon[1], G. Viesti[1], D. Bazzacco[1], D. Fabris[1], G. Nebbia[1], C. Ur[1], C. Rossi Alvarez[1], M. Cinausero[2,a], E. Farnea[2], E. Fioretto[2], G. Prete[2], G. de Angelis[2], D.R. Napoli[2], K. Hagel[3], J.B. Natowitz[3], and R. Wada[3]

[1] INFN and Dipartimento di Fisica di Padova, I-35131, Italy
[2] INFN, Laboratori Nazionali di Legnaro, I-35020 Legnaro, Italy
[3] Cyclotron Institute, Texas A&M University, College Station, TX 77843, USA

Received: 27 September 2001 / Revised version: 29 December 2001
Communicated by R.A. Ricci

Abstract. The reactions ^{11}B + ^{198}Pt $\rightarrow$ ^{209}Bi* and ^{10}B + ^{198}Pt $\rightarrow$ ^{208}Bi* have been investigated by measuring low- and high-energy γ-rays and proton-γ coincidences. The nuclear temperature of the ^{208}Pb populated by first-chance proton emission from ^{209}Bi has been determined by using an unfolding technique. The extracted value, $T = 1.6 \pm 0.2$ MeV, is compared with predictions from various level density parametrisations in which the shell effects play different roles. The comparison shows that, as expected in this excitation energy range, the shell effects in ^{208}Pb are substantially washed out. Proton and high-energy γ-ray spectra as well as neutron average multiplicities have been also compared with predictions from Statistical Model calculations making use of a constant ($a = A/10\,\mathrm{MeV}^{-1}$) or an excitation-energy–dependent level density parameter. The obtained results demonstrate that the high-energy γ-rays are more sensitive than protons to the level density variation with the excitation energy. However, Statistical Model calculations fail in reproducing satisfactorily the line-shape of the experimental γ-ray spectra, suggesting that the actual knowledge of the level densities in the ^{208}Pb region is not sufficiently accurate.

PACS. 21.10.Re Collective levels – 25.70.Gh Compound nucleus – 27.60.+j $90 \leq A \leq 149$

1 Introduction

The nuclear level density has been experimentally studied in the past years for nuclei at low excitation energies ($E_x \leq 10$ MeV), where strong effects related to the shell structures have been evidenced [1]. The shell effects are supposed to be washed out as the excitation energy increases. In fact, the experimental average value of the level density parameter $a = A/8\,\mathrm{MeV}^{-1}$ [2] used in several Statistical Model calculations, gives, in most cases, a realistic description of the compound nucleus decay in the excitation energy range $E_x = 50$–100 MeV. On the contrary, it is expected that shell effects should play a relevant role at lower excitation energies for compound systems close to the shell closures. A detailed knowledge of the excitation energy level density dependence is then needed to model the decay of the latter systems. As an example, in the case of the ^{208}Pb nucleus, which exhibits the largest known shell effects, the level density parameter value is $a \sim 10\,\mathrm{MeV}^{-1}$ at low excitation energy, whereas its asymptotic high excitation energy value is about $a \sim 20\,\mathrm{MeV}^{-1}$.

[a] e-mail: cinausero@lnl.infn.it

In the work of Ignatyuk [3] an energy-dependent formula for the level density parameter $a = a(U)$ has been proposed

$$a(U) = \tilde{a}\left(1 - f(U)\frac{\delta W}{U}\right), \qquad (1)$$

where $U = E^* - \Delta_\mathrm{p}$ is the excitation energy corrected for the pairing contribution,

$$\delta W = M_\mathrm{exp}(Z,A) - M_\mathrm{LDM}(Z,A)$$

is the difference between the experimental and the liquid-drop model predicted mass values and $\tilde{a}$ is the asymptotic value of the level density parameter. The function $f(U)$ determines the damping of the shell effects as a function of the excitation energy.

The Ignatyuk ansatz has been included by Reisdorf in its parametrisation of the level densities [4]. This parametrisation is also available as an option in a revised version of the Statistical Model code CASCADE [5], so that its role can be directly verified by comparing model predictions with experimental observables. Basically, the Reisdorf parametrisation make use of few parameters to determine the function $a(U)$: the damping energy D, the radius parameter r_0 and the pairing cor-

rection ($\Delta_{\rm p} = p/A^{1/2}$). In the work of ref. [4], available experimental data are well reproduced with values $r_0 = 1.153 \pm 0.01$ fm, $p = 10.5 \pm 2$ and $D = 18.5$ MeV.

At higher excitation energies, experimental studies for $A \sim 160$ systems [6] have shown convincing evidence of a second level density transition at $E_x \sim 1.5$–2 MeV per nucleon. In this second transition, the parameter a reaches its Fermi-Gas value $a = A/14$ MeV^{-1}. Recently, a possible evidence for this transition towards the Fermi-Gas value has been also reported for nuclei in the $A \sim 200$ region at excitation energy larger than 100 MeV [7–9], as qualitatively predicted by calculations in which the temperature dependence of the nucleon effective mass is included [10]. In the ^{208}Pb nucleus, this effect should again bring the parameter a to the value $a \sim 15$ MeV^{-1}.

We report here on a new experimental study on the role played by shell effects in excited nuclei around ^{208}Pb. For this purpose, the fusion reactions ^{11}B + ^{198}Pt $\rightarrow^{209}$ Bi* and ^{10}B + ^{198}Pt $\rightarrow$ ^{208}Bi* at bombarding energies of $E_{\rm beam} = 55$–90 MeV have been investigated. The experiment was mainly designed to directly derive, by using an unfolding technique, the nuclear temperature of the ^{208}Pb excited nucleus populated in the first-chance proton emission from ^{209}Bi. The extracted nuclear temperature value can be used, in fact, to study the ^{208}Pb level density.

2 Experimental details

The experimental work has been carried out at the XTU Tandem facility of the Laboratori Nazionali di Legnaro. Beams of ^{11}B and ^{10}B with intensity up to $\sim$ 5 pnA were focused onto a 1 mg/cm^2 ^{198}Pt target, 98% enriched. Beam energies are listed in table 1. The main irradiations were performed at $E_{\rm Beam} = 75$ MeV (^{11}B) and $E_{\rm Beam} = 60$ MeV (^{10}B). Short runs were performed at all other beam energies to carried out an excitation function measurement.

For each irradiation, low energy (*i.e.* $E_\gamma \leq 4$ MeV) γ-rays were detected with the GASP spectrometer [11], which, in its standard configuration, consists of an array of 40 Compton suppressed HPGe detectors, positioned in 7 rings at different angles with respect to the beam direction, and of an inner ball made by 80 bismuth germanate (BGO) scintillators.

In the present experiment, two of the HPGe detectors of the spectrometer (at $\theta_{\rm lab} = 90°$ and 145°) have been replaced by large volume (10 cm × 10 cm) cylindrical BGO scintillators, temperature stabilized and gain monitored, in order to detect high-energy γ-rays. Both scintillators were positioned at 75 cm from the target. The time-of-flight technique, with the start signal given by the GASP inner ball, was used to discriminate γ-rays from neutron-induced signals. A complete description of the operation of the large BGO detectors in coincidence with the GASP spectrometer can be found in ref. [12].

The GASP spectrometer housed a reaction chamber of 34 cm diameter, where the 4π charged particles detector array ISIS was installed [13]. ISIS is composed of 40 ΔE-E Si-telescopes (130 μm and 1000 μm thickness, respectively). The measured efficiency for protons is $\epsilon \approx 70\%$. In the present experiment, the ISIS capability for proton energy measurement was up-graded by backing the telescopes at $\langle\theta_{\rm lab}\rangle \sim 34°$ with additional CsI(Tl) detectors. The CsI(Tl) scintillators were 5 mm thick, with an active area of 2.5 × 2.5 cm^2 and used photodiode read-out.

Table 1. List of beam energies used in the present experiment.

^{11}B	^{10}B
55 MeV	55 MeV
60 MeV	60 MeV
	65 MeV
70 MeV	
75 MeV	
80 MeV	
90 MeV	

Different types of event have been collected during the experiment:

1) γ-rays and light charged particles coincidences, defined as one ISIS detector in coincidence with at least two HPGe and 3 inner ball elements;
2) high-energy γ-ray events, defined by the coincidence of anyone of the two large BGO detectors with at least two HPGe and 3 inner ball elements;
3) "single" GASP events defined by the condition of at least 3 HPGe and 3 inner ball elements firing in coincidence.

In the case of the ^{11}B irradiation at 75 MeV, we collect 200×10^6 coincidence events between ISIS and GASP detectors whereas the corresponding coincidences with energetic protons in the CsI(Tl) scintillators yielded only 2.6×10^6 events. The statistics collected in the ^{10}B irradiation at 60 MeV was 150×10^6 and 0.9×10^6 events, respectively.

The ISIS ΔE-E silicon telescopes were calibrated in energy by using α radioactive sources, energy loss tables and the known detector thickness. The CsI(Tl) scintillator calibration for protons was obtained relatively to the energy loss measured in the first two silicon elements of the telescopes.

The calibration of the large-volume BGO detectors was performed using radioctive sources (^{88}Y and ^{56}Co) and the two γ transitions ($E_\gamma = 7.4$, 10.2 MeV) that originate from neutron capture reactions in the Ge isotopes of the crystals [14].

The final spectra of the two BGO were summed together to increase the statistics, after the correction for the Doppler shift.

In the off-line analysis, the HPGe data were used to build inclusive E_γ-E_γ matrices and E_γ-E_γ-E_γ cubes. Furthermore, cubes and matrices were also generated by using coincidences between the high-energy γ-rays measured in one of the two BGOs ($E_\gamma^{\rm BGO}$) and the low-energy γ-rays measured in HPGe detectors. The ISIS data were used to build E_γ-E_γ matrices in coincidence with protons or

alpha-particles as well as E_γ-$E_{\rm LP}$ matrices, where $E_{\rm LP}$ is the measured light-particle energy.

3 Experimental results

The motivation of the present experiment was the study of the level density in the ^{208}Pb nucleus. This is mainly pursued by an unfolding of the proton spectra presented in the subsect. 3.1. Moreover, a global test of the actual knowledge of the level density in this mass region is obtained by a direct comparison of Statistical Model predictions with experimental proton and high-energy γ-ray spectra, as discussed in the subsects. 3.2 and 3.3.

3.1 Nuclear temperature in ^{208}Pb nucleus at $E_x = 50$ MeV

The ^{11}B + ^{198}Pt reaction at 75 MeV bombarding energy populates the ^{209}Bi compound nucleus at an excitation energy $E_x = 68.1$ MeV, when the complete fusion reaction mechanism is considered. The average angular momentum, estimated from fusion systematics is $\langle J \rangle \sim 20\hbar$.

The ^{10}B irradiation was performed at $E_{\rm Beam} = 60$ MeV, so that the ^{208}Bi compound nucleus is populated at an excitation energy $E_x = 58.1$ MeV. The excitation energy difference $\Delta E_x = 10$ MeV corresponds to the mean energy dissipated in the emission of the first neutron during the ^{209}Bi decay. Therefore, the proton spectrum measured in the ^{10}B-induced reaction should correspond, on average, to the pxn events in the de-excitation chains of the ^{209}Bi compound nucleus when a neutron is emitted in the first step of the decay, followed by protons evaporated in the second or later steps of the decay chains. Background events due to 2pxn decay channels were excluded by gating in both reactions on characteristic γ-rays of Pb evaporation residues.

It is, however, worth mentioning that the average angular momentum for the ^{10}B-induced reaction estimated from the fusion systematic is $\langle J \rangle \sim 15\hbar$, lower than the one in the ^{11}B irradiation. The effect of this unavoidable angular-momentum mismatch has been studied with Statistical Model calculations. The results show that, in this case, the spectrum line-shape and the multiplicity of the emitted protons are scarcely sensitive to angular-momentum–induced effects. Consequently, the angular-momentum mismatch has been disregarded in the following analysis. As a first step of the data analysis, the choice of the right bombarding energies for the unfolding procedure has been verified looking to the yield distribution of the Bi evaporation residues populated in the dominant xn decay channels of the ^{11}B and ^{10}B reactions. Relative yields were obtained from the analysis of known Bi transitions [15] identified in the inclusive E_γ-E_γ matrices. Data are reported in fig. 1 and in table 2. As expected, the relative yields of the ^{202}Bi and ^{203}Bi nuclei are the same in the two reactions, whereas a difference exists in the case of the ^{204}Bi nucleus which is produced at higher partial waves, being consequently more sensitive to the above-discussed angular-momentum mismatch. The neutron multiplicities derived from the residue distributions are $\nu_{\rm n}^{^{11}{\rm B}} = 5.93$ and $\nu_{\rm n}^{^{10}{\rm B}} = 5.03$. The difference value $\Delta\nu_{\rm n} = 0.9$ is very close to the expectation ($\Delta\nu_{\rm n} = 1$).

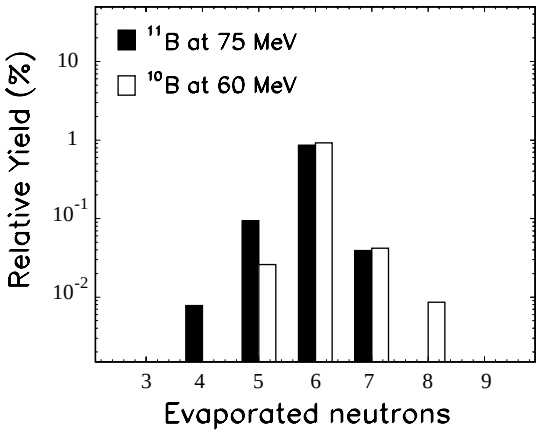

Fig. 1. Relative yields of the Bi isotopes populated in the 75 MeV ^{11}B + ^{198}Pt and 60 MeV ^{10}B + ^{198}Pt reactions. For the sake of comparison, the ^{10}B data have been shifted by + 1 neutron.

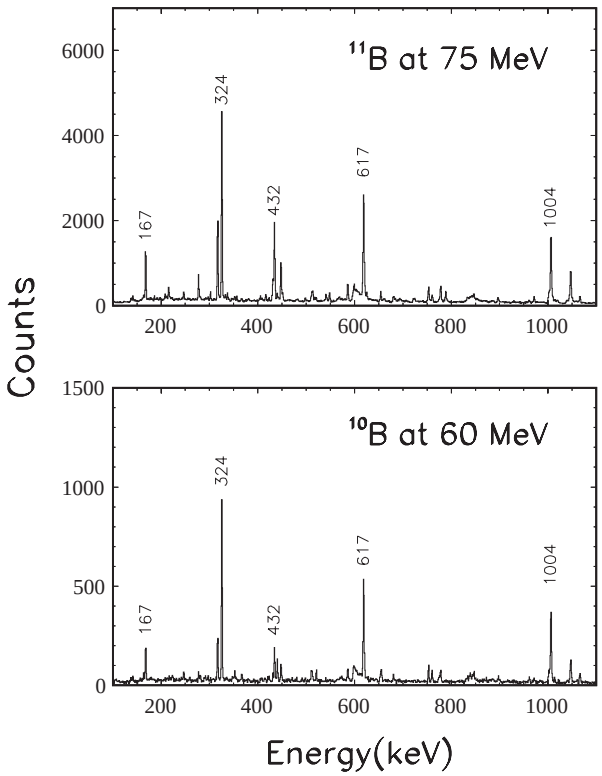

Fig. 2. Gamma-ray spectra in coincidence with energetic protons detected in the CsI(Tl) scintillators in the reactions of 75 MeV ^{11}B and 60 MeV ^{10}B on a ^{198}Pt target. The known transitions in the ^{204}Pb nucleus are indicated.

The E_γ-E_γ matrices obtained in coincidence with protons have been then used to look for the Pb isotopes populated in the pxn de-excitation channels. The nuclei ^{204}Pb, ^{203}Pb and ^{202}Pb were identified in the γ-ray spectra by

Table 2. Relative population of Bi ER (%).

Beam and Energy	^{201}Bi	^{202}Bi	^{203}Bi	^{204}Bi	^{205}Bi	^{205}Bi	ν_n
^{11}B at 55 MeV			2.1 ± 0.5	26 ± 5	72 ± 6	0.3 ± 0.1	4.29 ± 0.10
^{11}B at 60 MeV			3.2 ± 0.7	52 ± 7	45 ± 7		4.58 ± 0.10
^{11}B at 70 MeV		0.6 ± 0.2	68 ± 6	29 ± 6	1.9 ± 0.5		5.67 ± 0.12
^{11}B at 75 MeV		3.9 ± 1.2	86 ± 3	9 ± 2	0.8 ± 0.3		5.93 ± 0.05
^{11}B at 80 MeV	0.5 ± 0.2	16 ± 4	80 ± 4	3.1 ± 0.8			6.14 ± 0.12
^{11}B at 90 MeV	25 ± 5	51 ± 6	23 ± 4	1.0 ± 40.3			7.00 ± 0.10
^{10}B at 55 MeV	1.1 ± 0.4	0.5 ± 0.2	90 ± 2	8.3 ± 2			4.94 ± 0.07
^{10}B at 60 MeV	0.9 ± 0.3	4 ± 1	92 ± 2	2.6 ± 0.7			5.03 ± 0.05
^{10}B at 65 MeV	0.7 ± 0.2	31 ± 6	67 ± 6	1.2 ± 0.4			5.31 ± 0.07

Table 3. Relative population of Pb ER (%).

Beam and Energy	^{202}Pb	^{203}Pb	^{204}Pb	^{205}Pb	ν_n
^{11}B at 55 MeV			35 ± 7	65 ± 7	3.4 ± 0.4
^{11}B at 75 MeV	6 ± 2	44 ± 7	50 ± 7		4.6 ± 0.1
^{11}B at 90 MeV	21 ± 5	69 ± 6	10 ± 3		5.1 ± 0.5
^{10}B at 60 MeV	23 ± 6	50 ± 7	27 ± 6		3.96 ± 0.10

their known transitions [16]. Their relative yields are reported in table 3. As shown in fig. 2, protons with energies larger than 7 MeV, (*i.e.* hitting the CsI(Tl)) are mainly in coincidence with γ-ray transitions in the ^{204}Pb nucleus. The proton energy spectra in coincidences with transitions in different Pb evaporation residues are reported in figs. 3 and 4 for both reactions. The summed proton spectrum (SUM) is also shown. The SUM spectrum was obtained by adding the individual spectra weighted by the relative yields reported in table 3.

The apparent nuclear temperature parameter, $T_{\rm app}$, was derived for both reactions by a Maxwellian fit to the experimental proton spectra in coincidence with γ-ray transitions in ^{204}Pb, using the expression

$$Y(E) \propto (E - B_c) \exp\left[\frac{-(E - B_c)}{T_{\rm app}}\right],$$

where B_c is the average barrier. The fits were performed in the spectral region around 20 MeV considering only $T_{\rm app}$ as free parameter. We found $T_{\rm app}^{^{11}{\rm B}} = 1.24 \pm 0.09$ MeV and $T_{\rm app}^{^{10}{\rm B}} = 0.99 \pm 0.09$ MeV. The reported uncertainties take also into account small dependences of the best-fit values on the assumed average barrier ($B_c = 9.5 \pm 0.5$ MeV) and on the fitting region.

The relative yield of the decay channels ending in the ^{204}Pb nucleus was obtained for both reactions from the inclusive E_γ-E_γ matrix with respect to the sum of the evaporation residue yields. The relative yield values are found to be: $Y^{^{11}{\rm B}} = 8.05 \pm 0.30$ (a.u.) and $Y^{^{10}{\rm B}} = 4.93 \pm 0.23$ (a.u.).

Therefore, the temperature associated to the proton decay from the ^{209}Bi initial compound nucleus to the daughter ^{208}Pb nucleus in the first step of the p4n evaporation channel can be obtained from the measured apparent temperatures and relative yield as [17]

$$T(^{208}{\rm Pb}) = (Y^{^{11}{\rm B}} \times T_{\rm app}^{^{11}{\rm B}} - Y^{^{10}{\rm B}} \times T_{\rm app}^{^{10}{\rm B}})/(Y^{^{11}{\rm B}} - Y^{^{10}{\rm B}}) = 1.63 \pm 0.28\,{\rm MeV}\,.$$

The above temperature value is associated to a thermal excitation energy, $E_{\rm th}$, in the daughter ^{208}Pb nucleus given by

$$E_{\rm th} = E^*_{^{209}{\rm Bi}} - E^{\rm rot}_{^{208}{\rm Pb}} - S_{\rm p} - \langle E_{\rm p}^{\rm kin}\rangle = 49.5\,{\rm MeV}\,,$$

where $E^{\rm rot}_{^{208}{\rm Pb}}$ is the average rotational energy of the ^{208}Pb nucleus, $S_{\rm p}$ is the proton separation energy and $\langle E_{\rm p}^{\rm kin}\rangle$ is the average proton kinetic energy.

In fig. 5, our experimental temperature value is compared with predictions obtained from the Reisdorf level density parametrisation, (level density A), and with the two limiting values corresponding to a cold Pb nucleus where the shell corrections dominates ($a \sim 10$ MeV^{-1}) (level density B) and to an highly excited nucleus where such corrections are not present ($a \sim 20$ MeV^{-1}) (level density C). In the Reisdorf level density the original parameter values $r_0 = 1.153 \pm 0.01$ fm, $p = 10.5 \pm 2$ e $D = 18.5$ MeV from ref. [4] were used.

It appears that, at the excitation energy of $E_{\rm th} \sim 50$ MeV in the ^{208}Pb nucleus, the nuclear temperature is far from the value associated to the level density B), which characterizes the cold system. On the contrary, the experimental nuclear temperature is in agreement with the values associated to the Reisdorf parametrisation and to the asymptotic level density C). We note that the level density parameter in the Reisdorf approach has not yet reached, at this excitation energy, the asymptotic value C). However, the experimental uncertainty of our measurement does not allow a discrimination between them.

We note that, the result reported in fig. 5 is in agreement with the findings of a recent study of the reactions ^{207,208}Pb(n,xnγ) at neutron energies from 3 to 200 MeV

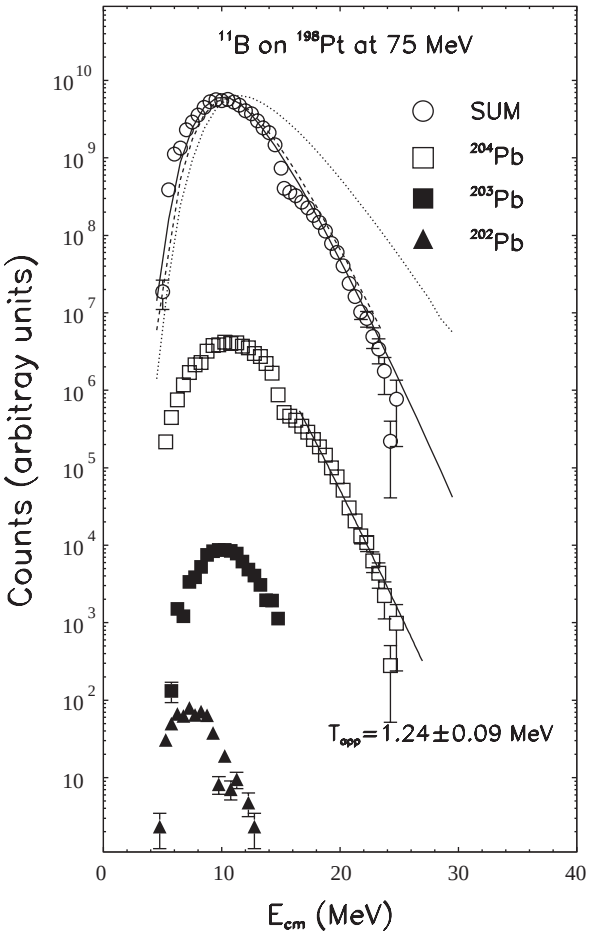

Fig. 3. Proton spectra from the 75 MeV ^{11}B + ^{198}Pt reaction measured in coincidence with discrete γ transitions in Pb evaporation residues. The SUM spectrum is obtained by summing with proper wheigts over all Pb residues. The SUM spectrum is compared with CASCADE statistical model calculations using the Reisdorf parametrization (full line) and the two limiting excitation energy-independent level density parameters: a = 10 MeV^{-1} (dotted line), a = 21 MeV^{-1} (dashed line). The Maxwellian fit results for the determination of $T_{\rm app}$ are also reported for the ^{204}Pb data. See text for more details.

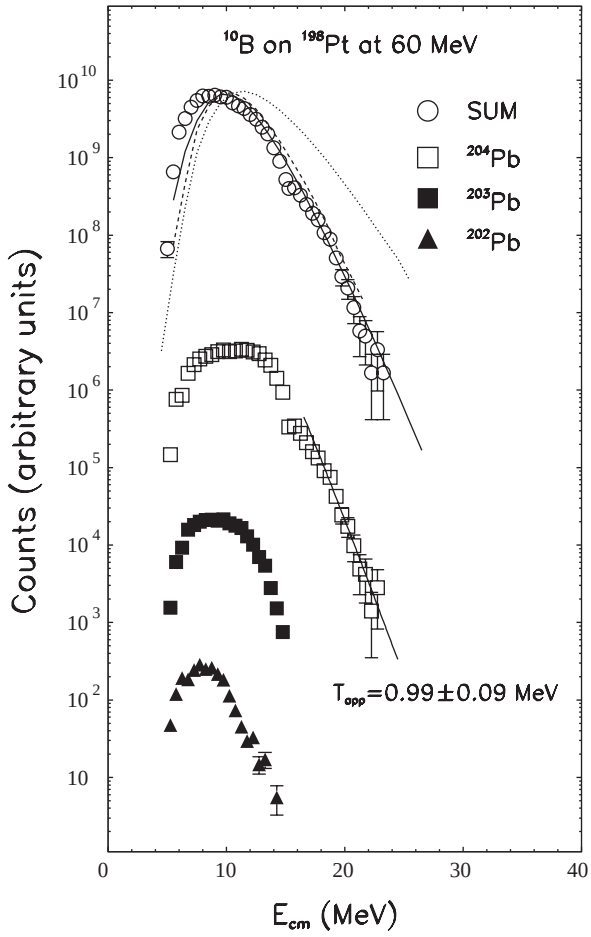

Fig. 4. As in fig. 3 but for the 60 MeV ^{10}B + ^{198}Pt reaction.

[18]. The analysis of the γ-ray production cross-sections with pre-equilibrium models, showed that level density parameter values around $a \sim 10$ MeV^{-1} should not be used at excitation energies larger than 30 MeV. In that work, a good description of the experimental data was obtained by using an excitation dependent level density parameter as predicted by Ignatiuk [3].

3.2 Comparison with Statistical Model calculations

As a further test of the level density of the nuclei around ^{208}Pb, the experimental data are compared in this section with Statistical Model (SM) predictions. Since the de-excitation chain involves several nuclei, the model calculations cannot be used to study the level density in a specific nucleus. However, the comparison between model predictions and experimental data allows a global test of the different level density prescriptions in the mass region around the ^{208}Pb nucleus. To this end, the CASCADE code was employed, using either the Reisdorf parametrisation A) or the constant level density parameters B) and C).

In fig. 6, the average neutron multiplicity $\nu_{\rm n}$ is compared with SM predictions. The experimental neutron multiplicities have been obtained from the relative yield distribution of the Bi isotopes produced in the dominant xn decay channels, as extracted from the γ-ray data (see subsect. 3.1). Calculations employing the level density A) give a very good account of the extracted experimental $\nu_{\rm n}$ in the explored bombarding energy range. This reflects the capability of the model to predict the relative distribution of the Bi isotopes at all bombarding energies. The same good description was also obtained for the experimental $\nu_{\rm n}$ in coincidence with one proton, *i.e.* associated to the Pb residue distribution.

In fig. 6, the experimental data are also compared with the predictions from calculations employing a constant level density B) and C). It is well known that the average kinetic energy of the emitted neutrons increases by decreasing the level density parameter value. Consequently, as shown in fig. 6, the predicted average number of neutrons is lower when the $a = A/21$ MeV^{-1} parameter value

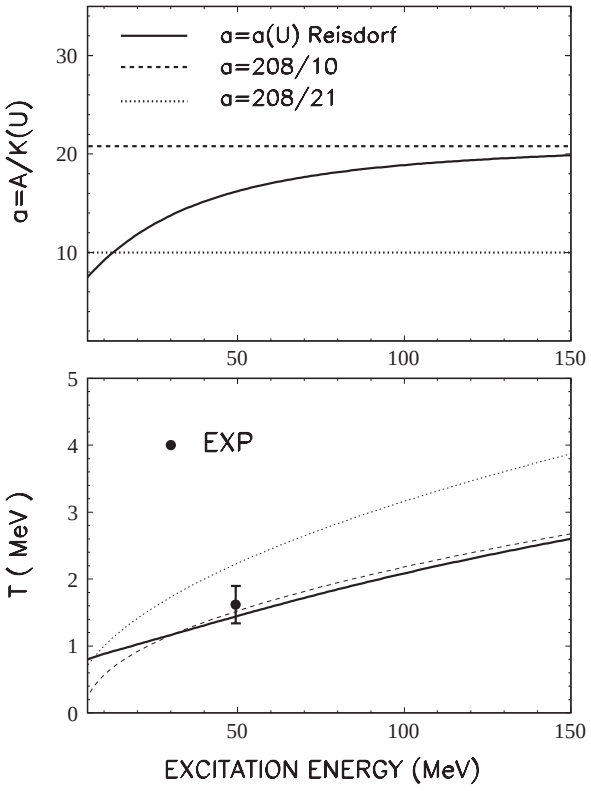

Fig. 5. Comparison of the experimental value for the nuclear temperture in ^{208}Pb with predictions using level density parametrisation A: Reisdorf, solid line, B: $a = A/K$, with $K = 21$ MeV, dotted line and C: $a = A/K$, $K = 10$ MeV, dashed line. See text for details.

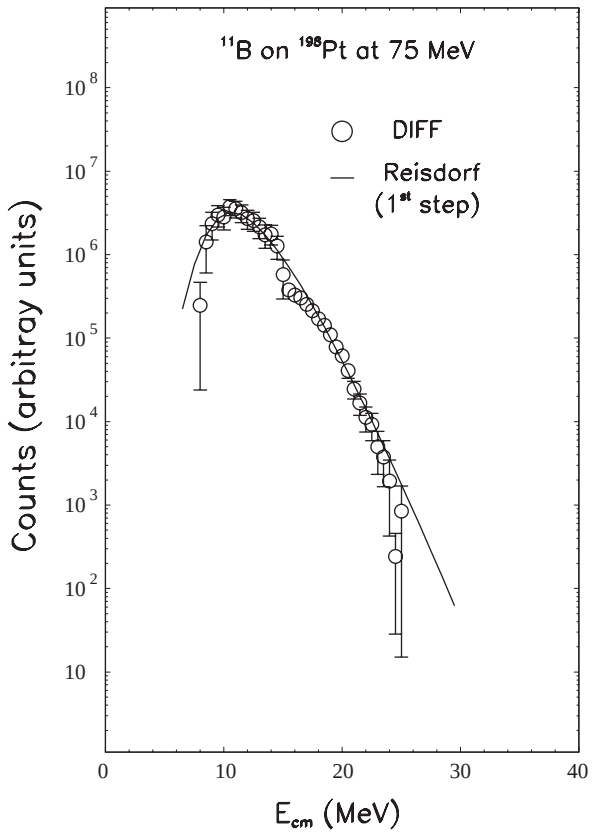

Fig. 7. Comparison between the experimental DIFF proton spectrum and the predicted first-chance proton energy distribution from Statistical Model calculations using the Reisdorf parametrisation A for the level density.

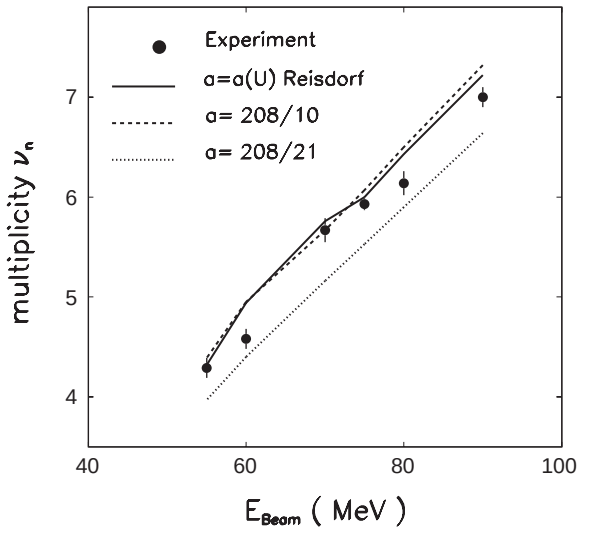

Fig. 6. Comparison between the experimental average neutron multiplicity derived from the γ-ray spectra and SM predictions using level density parametrizations A: Reisdorf, solid line, B: $a = A/K$, $K = 21$ MeV, dotted line and C: $a = A/K$, $K = 10$ MeV, dashed line. See text for details.

is used. The relevant fact in fig. 6 is that the calculations employing the constant level density parameter C) reproduce also well the experimental ν_n values.

Equivalent results are obtained when the experimental SUM proton spectra are compared with the SM predictions, as shown in figs. 3, 4. The calculated spectra using the Reisdorf parametrisation A) as well as the constant value C) are in nice agreement with the experimental spectra. On the contrary, the level density parameter B) predicts unrealistic energy spectra. It is important to stress that, following the SM predictions, protons contributing to the SUM spectra are mainly emitted at the higher excitation energies, where shell effects should not dominate. This, therefore, enhances the difference between calculations using the two asymptotic level densities B) and C).

A further constraint in the comparison between model prediction and experimental data is obtained by considering only the first-chance emitted protons. Experimentally, the first-chance spectrum (DIFF) has been obtained by subtracting the two SUM spectra from the ^{11}B- and ^{10}B-induced reactions. For this purpose, the spectra have been normalized to the measured relative yields from the E_γ-E_γ matrix. Therefore, as discussed at the beginning of subsect. 3.1, only the protons emitted in the ^{209}Bi decay branch that populates the ^{208}Pb excited nucleus should contribute to the DIFF spectrum. Also in this case, SM

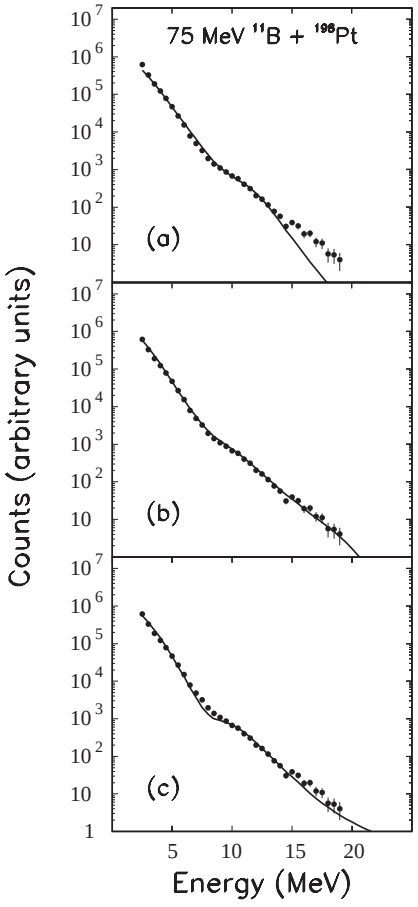

Fig. 8. High-energy γ-ray spectrum from the 75 MeV ^{11}B + ^{198}Pt reaction. Lines are Statistical Model fits to the data using a single Lorentzian distribution. Panels (a), (b), and (c) refer to the use of an excitation-energy–independent level density parameter $a = A/K$, with K value of 8, 10 and 21 MeV, respectively. Unrealistic GDR parameters are extracted from the fits, namely: for case (a) $S = 1.2$ (EWSR), $E_D = 12.2$ MeV, $\Gamma = 4.4$ MeV with $\chi^2/\nu = 6.9$, for case (b) $S = 0.95$ (EWSR), $E_D = 11.1$ MeV, $\Gamma = 6.5$ MeV with $\chi^2/\nu = 1.2$, for case (c) $S = 1.2$ (EWSR), $E_D = 10.4$ MeV, $\Gamma = 4.8$ MeV with $\chi^2/\nu = 1.9$. The estimated error for the strength S is ± 0.1 EWSR. For the centroid energy E_D and width Γ the estimated errors are ± 0.5 MeV.

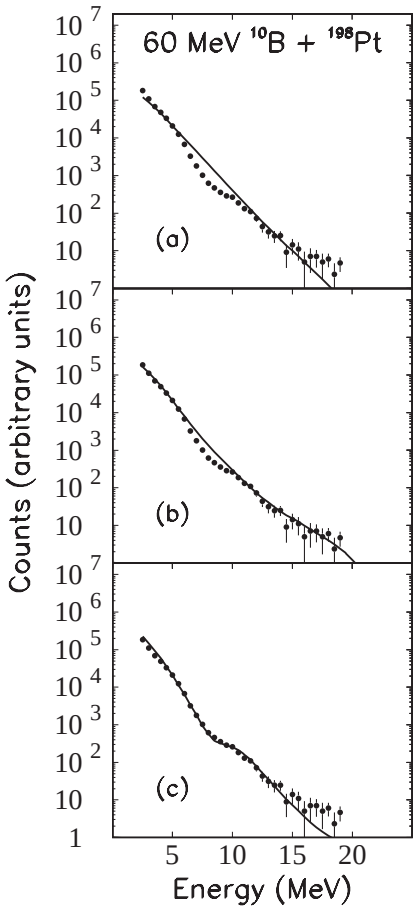

Fig. 9. As in fig. 8 but for the 60 MeV ^{10}B + ^{198}Pt reaction. Unrealistic GDR parameters are extracted from the fits, namely: for case (a) $S = 0.8$ (EWSR), $E_D = 9.0$ MeV, $\Gamma = 15.0$ MeV with $\chi^2/\nu = 9.4$, for case (b) $S = 1.0$ (EWSR), $E_D = 9.0$ MeV, $\Gamma = 9.4$ MeV with $\chi^2/\nu = 1.3$, for case (c) $S = 1.2$ (EWSR), $E_D = 10.6$ MeV, $\Gamma = 3.8$ MeV with $\chi^2/\nu = 2.2$. The estimated error for the strength S is ± 0.1 EWSR. For the centroid energy E_D and width Γ the estimated errors are ± 0.5 MeV.

predictions for the first-chance emitted protons using the level density A) accounts very well for the experimental DIFF spectrum as reported in fig. 7.

3.3 High-energy γ-ray spectra

The interest of the high-energy γ-ray measurement is related to the well-known fact [19] that the statistical tail of the spectrum at $E_\gamma \leq 8$ MeV is sensitive to the level density of the nuclei populated in the latest decay steps, where shell effects are magnified because of the low excitation energy. Therefore, the γ-ray spectrum line-shape should be a sensitive probe of the level density parametrisation used in the SM calculations.

The experimental γ-ray spectra measured in the two longer irradiations, ^{11}B at $E_{\rm beam} = 75$ MeV and ^{10}B at $E_{\rm beam} = 60$ MeV, are reported in figs. 8 and 9. The latter spectra have been obtained without any additional software condition with respect to the hardware trigger (see sect. 2). A Statistical Model fit to the data using the CASCADE code is also shown, assuming for simplicity a single Lorentzian distribution of the GDR strength function. Model calculations were performed with a constant level density parameter $a = A/K$ with $K = 8$, 10 and 21 MeV, respectively. The response function of the BGO detectors, obtained from the GEANT3 [20] code, was used to fold the SM predicted spectra. The extracted GDR parameters (strength S, centroid energy E_D and width Γ) are reported in the captions of figs. 8 and 9, together with the corresponding reduced χ^2 value of the fit.

Results indicate that the lowest χ^2 is achieved by using $K = 10$ MeV, *i.e.* the level density C). In the case

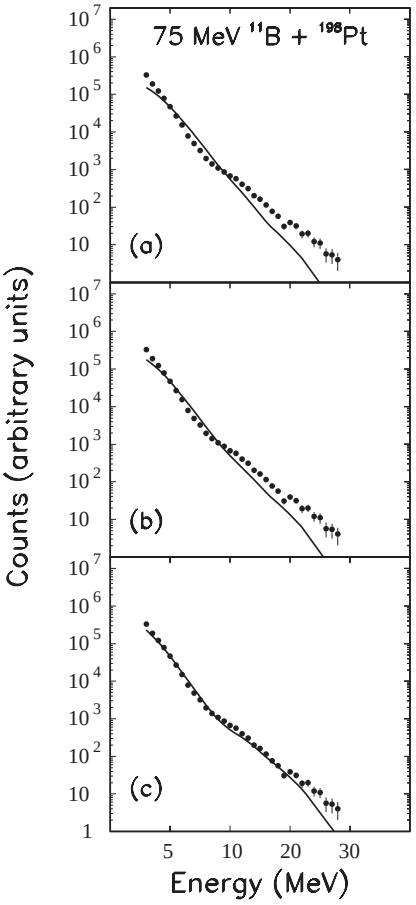

Fig. 10. Comparison of the experimental γ-ray spectrum from the 75 MeV ^{11}B + ^{198}Pt reaction with CASCADE Statistical Model calculations using the Reisdorf parametrisation for the level density. In panels (a), (b) and (c) damping energy parameters D = 14, 18.5 and 35 MeV are, respectively, employed. GDR parameter values from systematic in this mass region have been considered.

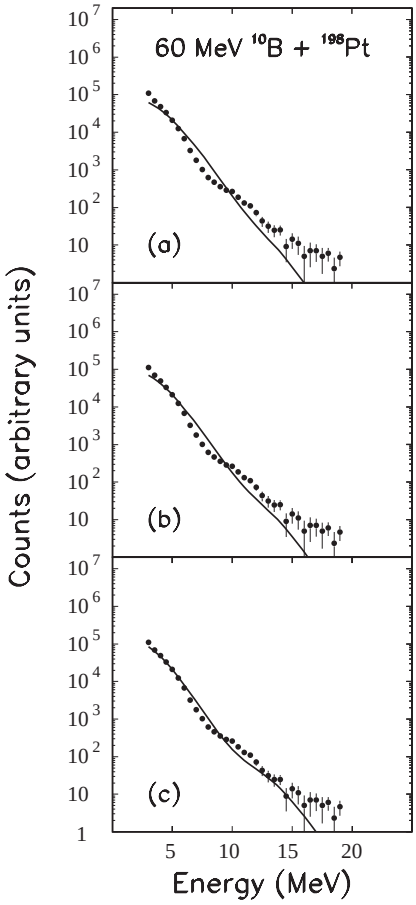

Fig. 11. As in fig. 10 but for the 60 MeV ^{10}B + ^{198}Pt reaction.

of the ^{11}B-induced reaction, model calculations provide a good fit over the entire spectrum. For the ^{10}B case, on the contrary, a better reproduction of the statistical part of the spectrum is obtained by using K = 21 MeV, *i.e.* the level density B). This should be qualitatively correlated to the lower excitation energy of the compound nucleus formed in the ^{10}B reaction.

The derived GDR parameters are not in agreement with systematics [21] and previous works in this mass and excitation energy range [22–24]. In particular, the GDR centroid energy is 2–3 MeV lower than expected. Similar discrepancies with previous findings resulted also from a more refined two-Lorentzian fit to the data. It seems, therefore, not possible to obtain realistic GDR parameters from a fitting procedure to the experimental γ-ray spectra in which constant level density parameters are used.

Consequently, we have performed Statistical Model calculations in which the Reisdorf level density is employed. In these calculations, GDR parameters were fixed to values extracted from previous works [21,23]: strength $S = 1$ EWSR, centroid energy E_D = 13.5 MeV and width Γ = 6.5 MeV. Different values of the damping parameter (D = 14, 18.5 and 35 MeV) have been considered. Results are compared with the experimental spectra in figs. 10 and 11 for the ^{11}B and ^{10}B reactions, respectively. Generally, it appears that the predicted spectra are quite sensitive to changes in the damping energy parameter values, showing that the shell effects play an important role for the description of the high-energy γ-ray spectrum lineshape in our excitation energy range. The best agreement between experimental and calculated spectra is achieved with the highest D value considered. As in the previous calculations, we observe that the γ-ray spectral shape is not completely accounted for in the ^{10}B case.

To further study the role of the shell corrections to the level density, we have here the possibility to compare the present high-energy γ-ray spectra with that obtained in the case of the neutron-deficient ^{200}Pb compound nucleus, extensively studied in the past [25,26]. The two nuclei ^{200}Pb and ^{209}Bi (or ^{208}Bi) are indeed quite different from the point of view of the shell corrections being the first one far from the shell closure.

In fig. 12 the γ spectrum from the reaction ^{19}F + ^{181}Ta at 101 MeV is reported [26], as measured with the same experimental set-up employed in the present work. This reactions populates the ^{200}Pb compound nucleus at an

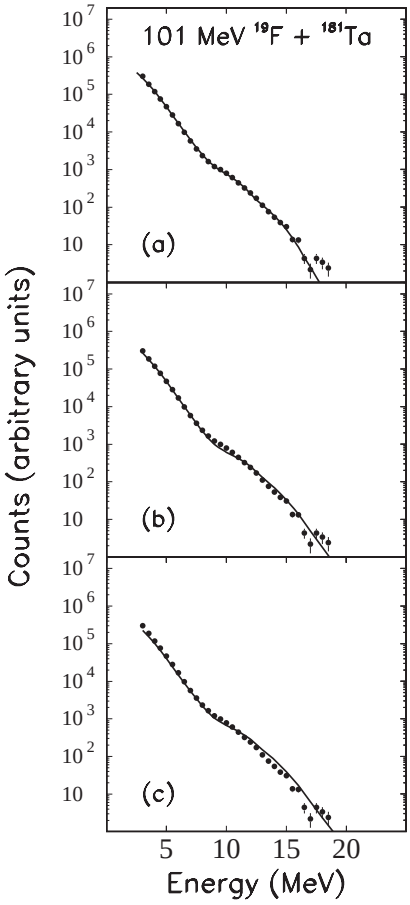

Fig. 12. Comparison of the experimental γ-ray spectrum from the 101 MeV ^{19}F + ^{181}Ta reaction with CASCADE Statistical Model calculations. In panel (a) a constant level density parameter $a = A/K$, with $K = 8$ MeV, is used. In panels (b) and (c) the Reisdorf parametrisation is employed with damping energy parameter $D = 14$ and 35 MeV, respectively. GDR parameter values are taken from ref. [24].

excitation energy close to that of the ^{209}Bi in the reaction ^{11}B + ^{198}Pt at 75 MeV. The experimental spectrum of fig. 12 is compared with the Statistical Model fit to the data obtained in ref. [26] using a two Lorentzian GDR strength distribution and a constant level density parameter $a = A/8$ MeV^{-1}. In the same figure, SM predictions using the Reisdorf level density with two values (*i.e.* $D = 14$ and 35 MeV) of the damping parameter, are also reported. In this case, calculations using both damping D values predict fairly well the experimental spectrum line-shape. This demonstrates that, as expected, the shell effects for nuclei around ^{200}Pb are strongly reduced with respect to the region in the vicinity of ^{209}Bi. In the latter case, indeed, the variation of the damping parameter D changes drastically the predicted spectrum.

Finally, it is interesting to comment on the difficulties in reproducing the high-energy γ-ray spectrum in case of the ^{10}B + ^{198}Pt reaction. As discussed in previous sections, the de-excitation chain of the ^{208}Bi compound nucleus populated in this reaction corresponds to the decay steps after the first neutron emission in the ^{209}Bi nucleus populated in the ^{11}B + ^{198}Pt reaction. This means that, with the already discussed partial angular-momentum overlap, the spectrum of the ^{10}B-induced reaction should correspond to part of that measured with the ^{11}B beam. The angular-momentum mismatch, however, should result in a difference on the average deformation of the two compound nuclei, influencing the width of the single Lorentzian GDR distribution as well as the resonance centroids in case of a two-Lorentzian fit. As already discussed, a good reproduction of the ^{10}B data is achieved only by using the level density B). In this case the GDR parameters of the two reactions are rather similar as far as the strength and resonance centroids it concerns . However, the GDR width of the ^{10}B is smaller with respect to that in the ^{11}B case, documenting the effects associated to the angular-momentum mismatch.

4 Summary and conclusions

In this work the nuclear temperature in the ^{208}Pb nucleus at about 50 MeV excitation energy has been derived by using an unfolding technique from the proton spectra measured in the ^{11}B- and ^{10}B-induced fusion reaction on a ^{198}Pt target.

The obtained value of the nuclear temperature has been compared with those resulting from different level density prescriptions: the Reisdorf excitation-energy–dependent parametrisation A) and the two excitation energy-independent limiting values for cold B) and hot C) ^{208}Pb nuclei. It is found that, within the uncertainties of the present measurement, the cold nucleus level density value is certainly ruled out, but it is not possible to discriminate between level density A) and C), *i.e.* to firmly establish the washing out of the the shell corrections in ^{208}Pb already at 50 MeV excitation energy.

An equivalent result is obtained by the direct comparison of the total and first-chance proton spectra with predictions from Statistical Model calculations in which the different level densities are used. The reduced sensitivity of the model calculations to the details of the level density is related to the fact that, in this mass region, protons are mainly emitted from nuclei at the highest excitation energies populated in the fusion reactions, whereas the bulk of the effects related to shell corrections is expected in nuclei at low excitation energy.

Furthermore, the comparison with Statistical Model calculations using different level density prescriptions shows that low excited nuclei along the decay chain play an important role in determining the line-shape of the measured high-energy gamma-ray spectra, being extremely sensitive to the detail of the assumed level density parametrisation. This has been also evidenced in a recent work by I. Dioszegi *et al.* [27] in which a comparative study of different level density prescriptions has been carried out in the mass region $A = 100$–140. The results obtained here for the ^{209,208}Bi compound nuclei have been compared with previous studies on the ^{200}Pb performed with the same experimental set up. In the latter case the

sensitivity to the detail of the different prescriptions is strongly reduced because the neutron-deficient nuclei involved in the de-excitation chain are far from the region where shell effects are maximised. The results obtained in case of the $^{11}B + ^{198}Pt$ and $^{19}F + ^{181}Ta$ reactions, which populate nuclei at the same excitation energy and with a rather similar range of angular momentum, clearly demonstrate the importance of the use of an excitation-energy–dependent parametrisation for the level density in nuclei near shell closures. The comparison between ^{11}B and ^{10}B data reveals, however, that the Reisdorf parametrisation needs to be improved for the nuclei at low excitation energy and at low angular momentum.

As a conclusion, results reported in this work indicate that an excitation-energy–dependent level density parametrisation should be important to model the decay of excited nuclear systems in the vicinity of the shell closure. The comparison of the experimental results with SM predictions might be used also to improve our knowledge on such effects. In this respect, it is important to select the most effective probe that samples all nuclei of the de-excitation chain. The high-energy γ-ray spectrum lineshape seems to be an useful tool for such investigations in the mass and excitation energy region explored in the present work.

References

1. A. Bohr, B.R. Mottelson, *Nuclear Structure*, Vol. **1** (Benjamin, New York, 1969).
2. R.G. Stokstadt, *Treatise on Heavy-Ion Science*, edited by D.A. Bromley, Vol. **3** (Plenum, New York, 1985) p. 83 and references therein.
3. A.V. Ignatyuk *et al.*, Sov. J. Nucl. Phys. **21**, 255 (1975).
4. W. Reisdorf, Z. Phys. A **300**, 227 (1981).
5. See M. Kicinska-Habior *et al.*, Phys. Rev. C **41**, 2075 (1990) and refrences therein.
6. M. Gonin *et al.*, Phys. Lett. B **217**, 406 (1989); Phys. Rev. C **42**, 2125 (1990) and references therein.
7. D. Fabris *et al.*, Phys. Rev. C **50**, 1261 (1994).
8. B.J. Fineman *et al.*, Phys. Rev. C **50**, 1991 (1994).
9. A.L. Caraley, B.P. Henry, J.P. Lestone, R. Vandenbosch, Phys. Rev. C **62**, 054612 (2000).
10. S. Shlomo, J.B. Natowitz, Phys. Rev. C **44**, 2878 (1991) and references therein.
11. D. Bazzacco *et al.*, Phys. Lett. B **309**, 235 (1993).
12. G. Viesti *et al.*, Nucl. Phys. A **604**, 81 (1996).
13. E. Farnea *et al.*, Nucl. Instrum. Methods Phys. Res. A **400**, 87 (1997).
14. W. Krolas, *et al.*, Z. Phys. A **344**, 147 (1992)
15. H. Hübel *et al.*, Nucl. Phys. A **294**, 177 (1978); A.P. Byrne *et al.*, Z. Phys. A **334**, 247 (1989); B.V.T. Rao *et al.*, Nucl. Phys. A **362**, 71 (1981); R. Broda *et al.*, Nucl. Phys. A **389**, 366 (1982); T. Lonnroth, Phys. Scr. **23**, 774 (1981); T. Lonnroth *et al.*, Z. Phys. A **287**, 307 (1978).
16. U. Rosengard *et al.*, Nucl. Phys. A **482**, 573 (1988); C.G. Linden, Z. Phys. A **284**, 217 (1978).
17. K. Hagel *et al.*, Nucl. Phys. A **486**, 429 (1988).
18. H. Vonach *et al.*, Phys. Rev. C **50**, 1952 (1994).
19. G. Feldman *et al.*, Phys. Rev. C **47**, 1436 (1993).
20. R. Brun, *et al.*, *GEANT3 Users Guide*, Data Handling Division, DD/EE/84-1, CERN (1986).
21. J.J. Gaardhøje, Annu. Rev. Nucl. Part. Sci. **42**, 483 (1992) and references therein.
22. E. Ramakrishnan *et al.*, Phys. Lett. B **383**, 252 (1996).
23. T. Baumann *et al.*, Nucl. Phys. A **653**, 428 (1998).
24. F. Camera *et al.*, Phys. Rev. C **60**, 14306 (1999).
25. D.R. Chakrabarty, M. Thoennessen, N. Alamanos, P. Paul, S. Sen, Phys. Rev. Lett. **58**, 1092 (1987).
26. N. Gelli *et al.*, Eur. Phys. J. A **7**, 361 (2000).
27. I. Dioszegi *et al.*, Phys. Rev. C **63**, 047601 (2000).